Search for anomalous production of events with a photon, jet, *b*-quark jet, and missing transverse energy

T. Aaltonen,[24] J. Adelman,[14] T. Akimoto,[56] B. Álvarez González,[12,r] S. Amerio,[44a,44b] D. Amidei,[35] A. Anastassov,[39] A. Annovi,[20] J. Antos,[15] G. Apollinari,[18] A. Apresyan,[49] T. Arisawa,[58] A. Artikov,[16] W. Ashmanskas,[18] A. Attal,[4] A. Aurisano,[54] F. Azfar,[43] P. Azzurri,[47a,47d] W. Badgett,[18] A. Barbaro-Galtieri,[29] V. E. Barnes,[49] B. A. Barnett,[26] V. Bartsch,[31] G. Bauer,[33] P.-H. Beauchemin,[34] F. Bedeschi,[47a] D. Beecher,[31] S. Behari,[26] G. Bellettini,[47a,47b] J. Bellinger,[60] D. Benjamin,[17] A. Beretvas,[18] J. Beringer,[29] A. Bhatti,[51] M. Binkley,[18] D. Bisello,[44a,44b] I. Bizjak,[31,w] R. E. Blair,[2] C. Blocker,[7] B. Blumenfeld,[26] A. Bocci,[17] A. Bodek,[50] V. Boisvert,[50] G. Bolla,[49] D. Bortoletto,[49] J. Boudreau,[48] A. Boveia,[11] B. Brau,[11,b] A. Bridgeman,[25] L. Brigliadori,[44a] C. Bromberg,[36] E. Brubaker,[14] J. Budagov,[16] H. S. Budd,[50] S. Budd,[25] S. Burke,[18] K. Burkett,[18] G. Busetto,[44b,44a] P. Bussey,[22] A. Buzatu,[34] K. L. Byrum,[2] S. Cabrera,[17,t] C. Calancha,[32] M. Campanelli,[36] M. Campbell,[35] F. Canelli,[14,18] A. Canepa,[46] B. Carls,[25] D. Carlsmith,[60] R. Carosi,[47a] S. Carrillo,[19,m] S. Carron,[34] B. Casal,[12] M. Casarsa,[18] A. Castro,[6b,6a] P. Catastini,[47a,47c] D. Cauz,[55a,55b] V. Cavaliere,[47a,47c] M. Cavalli-Sforza,[4] A. Cerri,[29] L. Cerrito,[31,n] S. H. Chang,[28] Y. C. Chen,[1] M. Chertok,[8] G. Chiarelli,[47a] G. Chlachidze,[18] F. Chlebana,[18] K. Cho,[28] D. Chokheli,[16] J. P. Chou,[23] G. Choudalakis,[33] S. H. Chuang,[53] K. Chung,[13] W. H. Chung,[60] Y. S. Chung,[50] T. Chwalek,[27] C. I. Ciobanu,[45] M. A. Ciocci,[47a,47c] A. Clark,[21] D. Clark,[7] G. Compostella,[44a] M. E. Convery,[18] J. Conway,[8] M. Cordelli,[20] G. Cortiana,[44a,44b] C. A. Cox,[8] D. J. Cox,[8] F. Crescioli,[47a,47b] C. Cuenca Almenar,[8,t] J. Cuevas,[12,r] R. Culbertson,[18] J. C. Cully,[35] D. Dagenhart,[18] M. Datta,[18] T. Davies,[22] P. de Barbaro,[50] S. De Cecco,[52a] A. Deisher,[29] G. De Lorenzo,[4] M. Dell'Orso,[47a,47b] C. Deluca,[4] L. Demortier,[51] J. Deng,[17] M. Deninno,[6a] P. F. Derwent,[18] G. P. di Giovanni,[45] C. Dionisi,[52a,52b] B. Di Ruzza,[55a,55b] J. R. Dittmann,[5] M. D'Onofrio,[4] S. Donati,[47a,47b] P. Dong,[9] J. Donini,[44a] T. Dorigo,[44a] S. Dube,[53] J. Efron,[40] A. Elagin,[54] R. Erbacher,[8] D. Errede,[25] S. Errede,[25] R. Eusebi,[18] H. C. Fang,[29] S. Farrington,[43] W. T. Fedorko,[14] R. G. Feild,[61] M. Feindt,[27] J. P. Fernandez,[32] C. Ferrazza,[47a,47d] R. Field,[19] G. Flanagan,[49] R. Forrest,[8] M. J. Frank,[5] M. Franklin,[23] J. C. Freeman,[18] H. J. Frisch,[14] I. Furic,[19] M. Gallinaro,[52a] J. Galyardt,[13] F. Garberson,[11] J. E. Garcia,[21] A. F. Garfinkel,[49] K. Genser,[18] H. Gerberich,[25] D. Gerdes,[35] A. Gessler,[27] S. Giagu,[52a,52b] V. Giakoumopoulou,[3] P. Giannetti,[47a] K. Gibson,[48] J. L. Gimmell,[50] C. M. Ginsburg,[18] N. Giokaris,[3] M. Giordani,[55a,55b] P. Giromini,[20] M. Giunta,[47a,47b] G. Giurgiu,[26] V. Glagolev,[16] D. Glenzinski,[18] M. Gold,[38] N. Goldschmidt,[19] A. Golossanov,[18] G. Gomez,[12] G. Gomez-Ceballos,[33] M. Goncharov,[33] O. González,[32] I. Gorelov,[38] A. T. Goshaw,[17] K. Goulianos,[51] A. Gresele,[44a,44b] S. Grinstein,[23] C. Grosso-Pilcher,[14] R. C. Group,[18] U. Grundler,[25] J. Guimaraes da Costa,[23] Z. Gunay-Unalan,[36] C. Haber,[29] K. Hahn,[33] S. R. Hahn,[18] E. Halkiadakis,[53] B.-Y. Han,[50] J. Y. Han,[50] F. Happacher,[20] K. Hara,[56] D. Hare,[53] M. Hare,[57] S. Harper,[43] R. F. Harr,[59] R. M. Harris,[18] M. Hartz,[48] K. Hatakeyama,[51] C. Hays,[43] M. Heck,[27] A. Heijboer,[46] J. Heinrich,[46] C. Henderson,[33] M. Herndon,[60] J. Heuser,[27] S. Hewamanage,[5] D. Hidas,[17] C. S. Hill,[11,d] D. Hirschbuehl,[27] A. Hocker,[18] S. Hou,[1] M. Houlden,[30] S.-C. Hsu,[29] B. T. Huffman,[43] R. E. Hughes,[40] U. Husemann,[61] M. Hussein,[36] J. Huston,[36] J. Incandela,[11] G. Introzzi,[47a] M. Iori,[52a,52b] A. Ivanov,[8] E. James,[18] D. Jang,[13] B. Jayatilaka,[17] E. J. Jeon,[28] M. K. Jha,[6a] S. Jindariani,[18] W. Johnson,[8] M. Jones,[49] K. K. Joo,[28] S. Y. Jun,[13] J. E. Jung,[28] T. R. Junk,[18] T. Kamon,[54] D. Kar,[19] P. E. Karchin,[59] Y. Kato,[42] R. Kephart,[18] J. Keung,[46] V. Khotilovich,[54] B. Kilminster,[18] D. H. Kim,[28] H. S. Kim,[28] H. W. Kim,[28] J. E. Kim,[28] M. J. Kim,[20] S. B. Kim,[28] S. H. Kim,[56] Y. K. Kim,[14] N. Kimura,[56] L. Kirsch,[7] S. Klimenko,[19] B. Knuteson,[33] B. R. Ko,[17] K. Kondo,[58] D. J. Kong,[28] J. Konigsberg,[19] A. Korytov,[19] A. V. Kotwal,[17] M. Kreps,[27] J. Kroll,[46] D. Krop,[14] N. Krumnack,[5] M. Kruse,[17] V. Krutelyov,[11] T. Kubo,[56] T. Kuhr,[27] N. P. Kulkarni,[59] M. Kurata,[56] S. Kwang,[14] A. T. Laasanen,[49] S. Lami,[47a] S. Lammel,[18] M. Lancaster,[31] R. L. Lander,[8] K. Lannon,[40,q] A. Lath,[53] G. Latino,[47a,47c] I. Lazzizzera,[44a,44b] T. LeCompte,[2] E. Lee,[54] H. S. Lee,[14] S. W. Lee,[54,s] S. Leone,[47a] J. D. Lewis,[18] C.-S. Lin,[29] J. Linacre,[43] M. Lindgren,[18] E. Lipeles,[46] A. Lister,[8] D. O. Litvintsev,[18] C. Liu,[48] T. Liu,[18] N. S. Lockyer,[46] A. Loginov,[61] M. Loreti,[44a,44b] L. Lovas,[15] D. Lucchesi,[44a,44b] C. Luci,[52a,52b] J. Lueck,[27] P. Lujan,[29] P. Lukens,[18] G. Lungu,[51] L. Lyons,[43] J. Lys,[29] R. Lysak,[15] D. MacQueen,[34] R. Madrak,[18] K. Maeshima,[18] K. Makhoul,[33] T. Maki,[24] P. Maksimovic,[26] S. Malde,[43] S. Malik,[31] G. Manca,[30,f] A. Manousakis-Katsikakis,[3] F. Margaroli,[49] C. Marino,[27] C. P. Marino,[25] A. Martin,[61] V. Martin,[22,l] M. Martínez,[4] R. Martínez-Ballarín,[32] T. Maruyama,[56] P. Mastrandrea,[52a] T. Masubuchi,[56] M. Mathis,[26] M. E. Mattson,[59] P. Mazzanti,[6a] K. S. McFarland,[50] P. McIntyre,[54] R. McNulty,[30,k] A. Mehta,[30] P. Mehtala,[24] A. Menzione,[47a] P. Merkel,[49] C. Mesropian,[51] T. Miao,[18] N. Miladinovic,[7] R. Miller,[36] C. Mills,[23] M. Milnik,[27] A. Mitra,[1] G. Mitselmakher,[19] H. Miyake,[56] N. Moggi,[6a] C. S. Moon,[28] R. Moore,[18] M. J. Morello,[47a,47b] J. Morlock,[27] P. Movilla Fernandez,[18] J. Mülmenstädt,[29] A. Mukherjee,[18] Th. Muller,[27] R. Mumford,[26] P. Murat,[18] M. Mussini,[6b,6a] J. Nachtman,[18] Y. Nagai,[56] A. Nagano,[56] J. Naganoma,[56] K. Nakamura,[56] I. Nakano,[41] A. Napier,[57] V. Necula,[17] J. Nett,[60] C. Neu,[46,u]

M. S. Neubauer,[25] S. Neubauer,[27] J. Nielsen,[29,h] L. Nodulman,[2] M. Norman,[10] O. Norniella,[25] E. Nurse,[31] L. Oakes,[43] S. H. Oh,[17] Y. D. Oh,[28] I. Oksuzian,[19] T. Okusawa,[42] R. Orava,[24] K. Osterberg,[24] S. Pagan Griso,[44a,44b] E. Palencia,[18] V. Papadimitriou,[18] A. Papaikonomou,[27] A. A. Paramonov,[14] B. Parks,[40] S. Pashapour,[34] J. Patrick,[18] G. Pauletta,[55a,55b] M. Paulini,[13] C. Paus,[33] T. Peiffer,[27] D. E. Pellett,[8] A. Penzo,[55a] T. J. Phillips,[17] G. Piacentino,[47a] E. Pianori,[46] L. Pinera,[19] K. Pitts,[25] C. Plager,[9] L. Pondrom,[60] O. Poukhov,[16,a] N. Pounder,[43] F. Prakoshyn,[16] A. Pronko,[18] J. Proudfoot,[2] F. Ptohos,[18,j] E. Pueschel,[13] G. Punzi,[47a,47b] J. Pursley,[60] J. Rademacker,[43,d] A. Rahaman,[48] V. Ramakrishnan,[60] N. Ranjan,[49] I. Redondo,[32] P. Renton,[43] M. Renz,[27] M. Rescigno,[52a] S. Richter,[27] F. Rimondi,[6a,6b] L. Ristori,[47a] A. Robson,[22] T. Rodrigo,[12] T. Rodriguez,[46] E. Rogers,[25] S. Rolli,[57] R. Roser,[18] M. Rossi,[55a] R. Rossin,[11] P. Roy,[34] A. Ruiz,[12] J. Russ,[13] V. Rusu,[18] H. Saarikko,[24] A. Safonov,[54] W. K. Sakumoto,[50] O. Saltó,[4] L. Santi,[55a,55b] S. Sarkar,[52a,52b] L. Sartori,[47a] K. Sato,[18] A. Savoy-Navarro,[45] P. Schlabach,[18] A. Schmidt,[27] E. E. Schmidt,[18] M. A. Schmidt,[14] M. P. Schmidt,[61,a] M. Schmitt,[39] T. Schwarz,[8] L. Scodellaro,[12] A. Scribano,[47a,47c] F. Scuri,[47a] A. Sedov,[49] S. Seidel,[38] Y. Seiya,[42] A. Semenov,[16] L. Sexton-Kennedy,[18] F. Sforza,[47a] A. Sfyrla,[25] S. Z. Shalhout,[59] T. Shears,[30] P. F. Shepard,[48] M. Shimojima,[56,p] S. Shiraishi,[14] M. Shochet,[14] Y. Shon,[60] I. Shreyber,[37] A. Sidoti,[47a] P. Sinervo,[34] A. Sisakyan,[16] A. J. Slaughter,[18] J. Slaunwhite,[40] K. Sliwa,[57] J. R. Smith,[8] F. D. Snider,[18] R. Snihur,[34] A. Soha,[8] S. Somalwar,[53] V. Sorin,[36] J. Spalding,[18] T. Spreitzer,[34] P. Squillacioti,[47a,47c] M. Stanitzki,[61] R. St. Denis,[22] B. Stelzer,[34] O. Stelzer-Chilton,[34] D. Stentz,[39] J. Strologas,[38] G. L. Strycker,[35] D. Stuart,[11] J. S. Suh,[28] A. Sukhanov,[19] I. Suslov,[16] T. Suzuki,[56] A. Taffard,[25,g] R. Takashima,[41] Y. Takeuchi,[56] R. Tanaka,[41] M. Tecchio,[35] P. K. Teng,[1] K. Terashi,[51] J. Thom,[18,i] A. S. Thompson,[22] G. A. Thompson,[25] E. Thomson,[46] P. Tipton,[61] P. Ttito-Guzmán,[32] S. Tkaczyk,[18] D. Toback,[54] S. Tokar,[15] K. Tollefson,[36] T. Tomura,[56] D. Tonelli,[18] S. Torre,[20] D. Torretta,[18] P. Totaro,[55a,55b] S. Tourneur,[45] M. Trovato,[47a] S.-Y. Tsai,[1] Y. Tu,[46] N. Turini,[47a,47c] F. Ukegawa,[56] S. Vallecorsa,[21] N. van Remortel,[24,c] A. Varganov,[35] E. Vataga,[47a,47d] F. Vázquez,[19,m] G. Velev,[18] C. Vellidis,[3] M. Vidal,[32] R. Vidal,[18] I. Vila,[12] R. Vilar,[12] T. Vine,[31] M. Vogel,[38] I. Volobouev,[29,s] G. Volpi,[47a,47b] P. Wagner,[46] R. G. Wagner,[2] R. L. Wagner,[18] W. Wagner,[27,v] J. Wagner-Kuhr,[27] T. Wakisaka,[42] R. Wallny,[9] S. M. Wang,[1] A. Warburton,[34] D. Waters,[31] M. Weinberger,[54] J. Weinelt,[27] W. C. Wester III,[18] B. Whitehouse,[57] D. Whiteson,[46,g] A. B. Wicklund,[2] E. Wicklund,[18] S. Wilbur,[14] G. Williams,[34] H. H. Williams,[46] P. Wilson,[18] B. L. Winer,[40] P. Wittich,[18,i] S. Wolbers,[18] C. Wolfe,[14] T. Wright,[35] X. Wu,[21] F. Würthwein,[10] S. Xie,[33] A. Yagil,[10] K. Yamamoto,[42] J. Yamaoka,[17] U. K. Yang,[14,o] Y. C. Yang,[28] W. M. Yao,[29] G. P. Yeh,[18] J. Yoh,[18] K. Yorita,[58] T. Yoshida,[42] G. B. Yu,[50] I. Yu,[28] S. S. Yu,[18] J. C. Yun,[18] L. Zanello,[52a,52b] A. Zanetti,[55a] X. Zhang,[25] Y. Zheng,[9,e] and S. Zucchelli[6a,6b]

(CDF Collaboration)

[1]*Institute of Physics, Academia Sinica, Taipei, Taiwan 11529, Republic of China*
[2]*Argonne National Laboratory, Argonne, Illinois 60439, USA*
[3]*University of Athens, 157 71 Athens, Greece*
[4]*Institut de Fisica d'Altes Energies, Universitat Autonoma de Barcelona, E-08193, Bellaterra (Barcelona), Spain*
[5]*Baylor University, Waco, Texas 76798, USA*
[6a]*Istituto Nazionale di Fisica Nucleare Bologna, I-40127 Bologna, Italy*
[6b]*University of Bologna, I-40127 Bologna, Italy*
[7]*Brandeis University, Waltham, Massachusetts 02254, USA*
[8]*University of California, Davis, Davis, California 95616, USA*
[9]*University of California, Los Angeles, Los Angeles, California 90024, USA*
[10]*University of California, San Diego, La Jolla, California 92093, USA*
[11]*University of California, Santa Barbara, Santa Barbara, California 93106, USA*
[12]*Instituto de Fisica de Cantabria, CSIC-University of Cantabria, 39005 Santander, Spain*
[13]*Carnegie Mellon University, Pittsburgh, Pennsylvania 15213, USA*
[14]*Enrico Fermi Institute, University of Chicago, Chicago, Illinois 60637, USA*
[15]*Comenius University, 842 48 Bratislava, Slovakia;*
Institute of Experimental Physics, 040 01 Kosice, Slovakia
[16]*Joint Institute for Nuclear Research, RU-141980 Dubna, Russia*
[17]*Duke University, Durham, North Carolina 27708, USA*
[18]*Fermi National Accelerator Laboratory, Batavia, Illinois 60510, USA*
[19]*University of Florida, Gainesville, Florida 32611, USA*
[20]*Laboratori Nazionali di Frascati, Istituto Nazionale di Fisica Nucleare, I-00044 Frascati, Italy*
[21]*University of Geneva, CH-1211 Geneva 4, Switzerland*
[22]*Glasgow University, Glasgow G12 8QQ, United Kingdom*
[23]*Harvard University, Cambridge, Massachusetts 02138, USA*

[24]Division of High Energy Physics, Department of Physics, University of Helsinki and Helsinki Institute of Physics, FIN-00014, Helsinki, Finland
[25]University of Illinois, Urbana, Illinois 61801, USA
[26]The Johns Hopkins University, Baltimore, Maryland 21218, USA
[27]Institut für Experimentelle Kernphysik, Universität Karlsruhe, 76128 Karlsruhe, Germany
[28]Center for High Energy Physics: Kyungpook National University, Daegu 702-701, Korea;
Seoul National University, Seoul 151-742, Korea;
Sungkyunkwan University, Suwon 440-746, Korea;
Korea Institute of Science and Technology Information, Daejeon, 305-806, Korea;
Chonnam National University, Gwangju, 500-757, Korea
[29]Ernest Orlando Lawrence Berkeley National Laboratory, Berkeley, California 94720, USA
[30]University of Liverpool, Liverpool L69 7ZE, United Kingdom
[31]University College London, London WC1E 6BT, United Kingdom
[32]Centro de Investigaciones Energeticas, Medioambientales y Tecnologicas, E-28040 Madrid, Spain
[33]Massachusetts Institute of Technology, Cambridge, Massachusetts 02139, USA
[34]Institute of Particle Physics: McGill University, Montréal, Québec, Canada H3A 2T8;
Simon Fraser University, Burnaby, British Columbia, Canada V5A 1S6;
University of Toronto, Toronto, Ontario, Canada M5S 1A7;
and TRIUMF, Vancouver, British Columbia, Canada V6T 2A3
[35]University of Michigan, Ann Arbor, Michigan 48109, USA
[36]Michigan State University, East Lansing, Michigan 48824, USA
[37]Institution for Theoretical and Experimental Physics, ITEP, Moscow 117259, Russia
[38]University of New Mexico, Albuquerque, New Mexico 87131, USA
[39]Northwestern University, Evanston, Illinois 60208, USA
[40]The Ohio State University, Columbus, Ohio 43210, USA
[41]Okayama University, Okayama 700-8530, Japan
[42]Osaka City University, Osaka 588, Japan
[43]University of Oxford, Oxford OX1 3RH, United Kingdom
[44a]Istituto Nazionale di Fisica Nucleare, Sezione di Padova-Trento, I-35131 Padova, Italy
[44b]University of Padova, I-35131 Padova, Italy
[45]LPNHE, Universite Pierre et Marie Curie/IN$_2$P$_3$-CNRS, UMR7585, Paris, F-75252 France
[46]University of Pennsylvania, Philadelphia, Pennsylvania 19104, USA
[47a]Istituto Nazionale di Fisica Nucleare Pisa, I-56127 Pisa, Italy
[47b]University of Pisa, I-56127 Pisa, Italy
[47c]University of Siena, I-56127 Pisa, Italy
[47d]Scuola Normale Superiore, I-56127 Pisa, Italy
[48]University of Pittsburgh, Pittsburgh, Pennsylvania 15260, USA
[49]Purdue University, West Lafayette, Indiana 47907, USA
[50]University of Rochester, Rochester, New York 14627, USA

[a]Deceased.

[b]Visitor from University of Massachusetts Amherst, Amherst, MA 01003, USA.

[c]Visitor from Universiteit Antwerpen, B-2610 Antwerp, Belgium.

[d]Visitor from University of Bristol, Bristol BS8 1TL, United Kingdom.

[e]Visitor from Chinese Academy of Sciences, Beijing 100864, China.

[f]Visitor from Istituto Nazionale di Fisica Nucleare, Sezione di Cagliari, 09042 Monserrato (Cagliari), Italy.

[g]Visitor from University of California Irvine, Irvine, CA 92697, USA.

[h]Visitor from University of California Santa Cruz, Santa Cruz, CA 95064, USA.

[i]Visitor from Cornell University, Ithaca, NY 14853, USA.

[j]Visitor from University of Cyprus, Nicosia CY-1678, Cyprus.

[k]Visitor from University College Dublin, Dublin 4, Ireland.

[l]Visitor from University of Edinburgh, Edinburgh EH9 3JZ, United Kingdom.

[m]Visitor from Universidad Iberoamericana, Mexico D.F.,

[n]Visitor from Queen Mary, University of London, London, E1 4NS, United Kingdom.

[o]Visitor from University of Manchester, Manchester M13 9PL, United Kingdom.

[p]Visitor from Nagasaki Institute of Applied Science, Nagasaki, Japan.

[q]Visitor from University of Notre Dame, Notre Dame, IN 46556, USA.

[r]Visitor from University de Oviedo, E-33007 Oviedo, Spain.

[s]Visitor from Texas Tech University, Lubbock, TX 79409, USA.

[t]Visitor from IFIC (CSIC-Universitat de Valencia), 46071 Valencia, Spain.

[u]Visitor from University of Virginia, Charlottesville, VA 22904, USA.

[v]Visitor from Bergische Universität Wuppertal, 42097 Wuppertal, Germany.

[w]On leave from J. Stefan Institute, Ljubljana, Slovenia.

[51]*The Rockefeller University, New York, New York 10021, USA*
[52a]*Istituto Nazionale di Fisica Nucleare, Sezione di Roma 1, I-00185 Roma, Italy*
[52b]*Sapienza Università di Roma, I-00185 Roma, Italy*
[53]*Rutgers University, Piscataway, New Jersey 08855, USA*
[54]*Texas A&M University, College Station, Texas 77843, USA*
[55a]*Istituto Nazionale di Fisica Nucleare Trieste/Udine, I-34100 Trieste, I-33100 Udine, Italy*
[55b]*University of Trieste/Udine, I-33100 Udine, Italy*
[56]*University of Tsukuba, Tsukuba, Ibaraki 305, Japan*
[57]*Tufts University, Medford, Massachusetts 02155, USA*
[58]*Waseda University, Tokyo 169, Japan*
[59]*Wayne State University, Detroit, Michigan 48201, USA*
[60]*University of Wisconsin, Madison, Wisconsin 53706, USA*
[61]*Yale University, New Haven, Connecticut 06520, USA*
(Received 2 May 2009; published 14 September 2009)

We present a signature-based search for the anomalous production of events containing a photon, two jets, of which at least one is identified as originating from a b quark, and missing transverse energy ($\not\!\!E_T$). The search uses data corresponding to 2.0 fb^{-1} of integrated luminosity from $p\bar{p}$ collisions at a center-of-mass energy of $\sqrt{s} = 1.96$ TeV, collected with the CDF II detector at the Fermilab Tevatron. From $6.697\,47 \times 10^6$ events with a photon candidate with transverse energy $E_T > 25$ GeV, we find 617 events with $\not\!\!E_T > 25$ GeV and two or more jets with $E_T > 15$ GeV, at least one identified as originating from a b quark, versus an expectation of 607 ± 113 events. Increasing the requirement on $\not\!\!E_T$ to 50 GeV, we find 28 events versus an expectation of 30 ± 11 events. We find no indications of non-standard-model phenomena.

DOI: 10.1103/PhysRevD.80.052003 PACS numbers: 13.85.Qk, 12.60.Jv, 14.80.Ly

I. INTRODUCTION

Within the standard model of elementary particle physics (SM), there are six flavors of quarks, six flavors of leptons, and four vector gauge bosons, with a hierarchy of couplings and masses. The Fermilab Tevatron, with a center-of-mass energy of 1.96 TeV, can produce all of the known quarks and vector bosons. Over the course of years of data-taking using the CDF detector [1], we have developed a suite of largely data-driven methods by which we estimate the efficiencies and backgrounds associated with the identification of charged leptons, heavy-flavor quarks (b or c quarks), electroweak gauge bosons (photons, $W^{\pm}$, and Z^0), and the presence of neutrinos, identified generically by missing transverse energy ($\not\!\!E_T$) [2]. The ability to identify these ''objects'' in events and to estimate their efficiencies and backgrounds has led to the development of signature-based searches at the Tevatron, in which one defines *a priori* the objects an event is required to contain, and then compares observations to expectations [3–9]. The model tested in these searches is the SM, which is predictive and falsifiable; any deviation from the SM predictions would be a signal of new phenomena. The advantage of this strategy is that only once such a signal has been established would the investment be made in generating detailed predictions of the many possible models for the new phenomena.

We describe here a search for new physics in the inclusive $\gamma bj\not\!\!E_T$ channel using 2.0 ± 0.1 fb^{-1} of integrated luminosity at a center-of-mass energy of $\sqrt{s} = 1.96$ TeV, collected between February 2002 and May 2007. A similar search was originally performed in run I using ≈ 85 pb^{-1} of integrated luminosity [10]. Our search in run II is part of a broad effort at CDF to study rare event signatures involving photons for any non-SM sources [6–8]. The SM processes, either with a radiated photon or where the charged lepton is misidentified as a photon, are expected to contribute $\approx 2\%$ ($t\bar{t} \to \ell\bar{\nu}jjb\bar{b}$) and $<1\%$ ($Wb\bar{b} \to \ell\bar{\nu}b\bar{b}$ and $Zb\bar{b} \to \nu\bar{\nu}b\bar{b}$) to the measured rate [11]. Because the SM contributions to the $\gamma bj\not\!\!E_T$ final state are highly suppressed, for an ideal detector the signature provides an excellent place to look for new phenomena. In reality, we expect additional events from processes such as γ + jets and $b\bar{b}$ production in which mismeasurements of the jet energy induce $\not\!\!E_T$.

The outline of the paper is as follows. Section II briefly describes the CDF II detector. The selection of events with photons, jets, jets from a heavy-flavor quark (b or c quark), and missing transverse energy is described in Sec. III. The estimation of backgrounds to the search sample is presented in Sec. IV. Section V describes the sources and estimates of systematic uncertainties on the numbers of events from backgrounds. The results of the search, including the effect of additional selection criteria and the efficiencies necessary for calculating limits, are presented in Sec. VI. Section VII presents the conclusions.

II. THE CDF II DETECTOR

The CDF II detector is a cylindrically symmetric spectrometer designed to study $\bar{p}p$ collisions at the Fermilab Tevatron. The detector has been extensively described in

detail in the literature [1]. Here we briefly describe the detector subsystems relevant for the analysis.

Tracking systems are used to measure the momenta of charged particles, to reconstruct primary and secondary vertices, and to trigger on and identify leptons with large transverse momentum [2]. Silicon strip detectors [12] and the central outer tracker (COT) [13] are contained in a superconducting solenoid that generates a magnetic field of 1.4 T. The silicon strip system provides up to eight measurements in the $r-\phi$ and $r-z$ views [2] and covers the track reconstruction in the region $|\eta| < 2$. The COT is an open-cell drift chamber that makes up to 96 measurements along the track of each charged particle in the region $|\eta| < 1$. Sense wires are arranged in eight alternating axial and $\pm 2^\circ$ stereo superlayers. The resolution in p_T, σ_{p_T}/p_T, is $\approx 0.0015 p_T \cdot \mathrm{GeV}^{-1} \cdot c$ for tracks with only COT measurements, and $\approx 0.0007 p_T \cdot \mathrm{GeV}^{-1} \cdot c$ for tracks with both the silicon and COT measurements.

Calorimeters are segmented with towers arranged in a projective geometry. Each tower consists of an electromagnetic and a hadronic compartment [14–16], covering the central region, $|\eta| < 1.1$, and the "end plug" region, $1.1 < |\eta| < 3.6$. The central electromagnetic calorimeter (CEM) and central hadronic calorimeter (CHA) are in the central region while the plug electromagnetic calorimeter (PEM) and plug hadronic calorimeter (PHA) are in the end plug region. In this analysis, a high-E_T photon is required to be identified in the central region, where the CEM has a segmentation of 15° in ϕ and ≈ 0.1 in η [1], and an E_T resolution of $\sigma(E_T)/E_T \approx 13.5\%/\sqrt{E_T/\mathrm{GeV}} \oplus 2\%$ [14]. We further require a high-E_T jet to be identified in the central region, where the jet energy resolution is approximately $\sigma \approx 0.1 \cdot E_T\ (\mathrm{GeV}) \oplus 1.0\ \mathrm{GeV}$ [17]. Two additional systems in the central region with finer spatial resolution are used for photon identification in this analysis. The central strip system, CES, uses a multiwire proportional chamber with 1.67- and 2.01-cm-wide cathode strips and a wire spacing of 1.45 cm to make profile measurements of electromagnetic showers at a depth of 6 radiation lengths (approximately the shower maximum). The central preshower detector, CPR, located just outside the solenoid coil on the front face of the CEM, separates single photons from the photon pairs from π^0 and η^0 decays on a statistical basis, as described in Sec. IV A. In 2005 the CPR was upgraded from the run I configuration of wire proportional chambers, similar to those used in the CES, to a fast scintillator system with a segmentation of 12.5 cm in ϕ and 12.5 cm in z [16]. The finer segmentation in z reduces the probability of a random hit from the underlying event and multiple interactions by a factor of 4, thereby improving the performance of the preshower detector in higher luminosity beam conditions.

Muons are identified using the central muon systems [18]: CMU and CMP for the pseudorapidity region of $|\eta| < 0.6$, and CMX for the pseudorapidity region of $0.6 < |\eta| < 1.0$. The CMU system uses four layers of planar drift chambers to detect muons with $p_T > 1.4\ \mathrm{GeV}/c$. The CMP system consists of an additional four layers of planar drift chambers located behind 0.6 m of steel outside the magnetic return yoke, and detects muons with $p_T > 2.2\ \mathrm{GeV}/c$. The CMX system detects muons with $p_T > 1.4\ \mathrm{GeV}/c$ with four to eight layers of drift chambers, depending on the direction of the muon.

The luminosity is measured using two sets of gas Cerenkov counters [19], located in the region $3.7 < |\eta| < 4.7$. The total uncertainty on the luminosity is estimated to be 5.9%, where 4.4% comes from the acceptance and operation of the luminosity monitor and 4.0% from the calculation of the inelastic $\bar{p}p$ cross section [20].

A three-level trigger system [21] selects events to be recorded for further analysis. The first two trigger levels consist of dedicated fast digital electronics analyzing a subset of the full detector data. The third level, applied to the full data of those events passing the first two levels, consists of a farm of computers that reconstruct the data and apply selection criteria consistent with the subsequent offline event processing.

III. EVENT SELECTION

An initial sample of events enhanced with high energy photons is collected using a trigger that requires a high energy isolated cluster in the electromagnetic calorimeter [22]. We require events to have a primary vertex with $|z| < 60$ cm. The offline selection criteria require a central ($|\eta| < 1.1$) photon with $E_T > 25$ GeV, two jets with $|\eta| < 2.0$ and $E_T > 15$ GeV, at least one of which is identified as originating from a b quark (b-tagged), and missing transverse energy greater than 25 GeV, as described in more detail below. The selection is inclusive; i.e. we allow extra objects (jets, photons, leptons) in the events.

The photon is required to satisfy the same identification requirements as in previous CDF high-E_T photon analyses [23]. Namely, the photon candidate is required to have no associated track with $p_T > 1$ GeV, at most one track with $p_T < 1$ GeV pointing at the calorimeter cluster [24], good profiles of electromagnetic energy measured in both transverse dimensions at the shower maximum, and minimal leakage into the hadron calorimeter [25]. Photon candidates identified via these cuts are referred to as "standard" photons.

Jets are reconstructed using the JETCLU cone algorithm [26] with cone radius $R = \sqrt{\Delta\phi^2 + \Delta\eta^2} = 0.4$. Starting from seed locations corresponding to calorimeter towers with $E_T > 1$ GeV, all nearby towers with $E_T > 0.1$ GeV are used to search for stable cones. To resolve ambiguities with overlapping cones, cones sharing an energy fraction greater than 0.75 are merged into a single jet; otherwise the shared towers are assigned to the closest jet. We apply a jet energy scale (JES) correction [27] such that the measured E_T is, on average, equal to the summed E_T of the particles

TABLE I. Summary of the event selection. The selection of a central photon includes the requirement of the inclusive photon trigger, the selections on the z vertex, and $E_T(\gamma)$ as described in Sec. III. The selection $\Delta R > 0.4$ is required for each pair of γj_1, γj_2, and $j_1 j_2$.

Cut	Events
Photon with $E_T > 25$ GeV, $\|\eta\| < 1.1$	$6.697\,47 \times 10^6$
Two jets with $E_T > 15$ GeV, $\|\eta\| < 2.0$	$1.944\,96 \times 10^6$
$\Delta R > 0.4$ for γj_1, γj_2, and $j_1 j_2$	$1.941\,34 \times 10^6$
$\not\!\!E_T \geq 25$ GeV	35 463
$\Delta\phi(\text{jet}, \not\!\!E_T) > 0.3$	18 128
≥ 1 SECVTX b-tag	617

from the $p\bar{p}$ interaction within the jet cone. At least one of the jets must be b-tagged using the SECVTX algorithm [28], which searches for displaced vertices using the reconstructed tracks inside the jet cone.

Missing transverse energy $\not\!\!E_T$ is calculated [2] from the calorimeter tower energies in the region $|\eta| < 3.6$. Corrections are then applied to the $\not\!\!E_T$ for (i) the calorimeter response for identified jets [27] and (ii) the presence of muons with $p_T > 20$ GeV. We require the corrected $\not\!\!E_T$ to be greater than 25 GeV and minimize the number of events with mismeasured $\not\!\!E_T$ by requiring the difference in azimuthal angle between any jet and the $\not\!\!E_T$, $\Delta\phi(\text{jet}, \not\!\!E_T)$, to be greater than 0.3. The requirement $\Delta R > 0.4$ is imposed on all combinations of the photon and the two selected jets, namely, γj_1, γj_2, and $j_1 j_2$. One of the two jets is the leading b-tagged jet, and the other is the next-to-leading b-tagged jet if one exists, or the leading non-b-tagged jet if not.

Table I summarizes the event selection. The final $\gamma b j \not\!\!E_T$ sample with $\not\!\!E_T > 25$ GeV corresponds to one part in 10^4 of inclusive high-E_T photon events. We will refer to this sample of 617 events as the ''search'' sample.

IV. BACKGROUND PREDICTIONS

To understand the composition of the search sample of 617 events, we could, in principle, use Monte Carlo (MC) simulations to estimate the absolute numbers of events with real or misidentified photons, and real or misidentified heavy flavor. However, this method would result in large systematic uncertainties on the number of events due to theoretical uncertainties on the production cross sections and difficulties in modeling misidentifications. We have consequently developed a data-driven strategy that uses the Monte Carlo simulation judiciously to minimize systematic uncertainties.

As mentioned in Sec. I, SM processes with final state neutrinos are not expected to contribute significantly to the search region. We check this expectation by vetoing events that have any high-p_T isolated tracks, effectively removing any contribution from processes involving leptonic decays of vector bosons. Isolated tracks are defined as tracks with $p_T > 20$ GeV having an isolation fraction larger than 0.9, where the isolation fraction is defined as

$$f_{\text{iso}} = \frac{p_T^{\text{track}}}{p_T^{\text{track}} + \sum_i p_T^i}.$$

Further details of the isolation calculation are given in Ref. [29]. After the application of the isolated track veto, the observed number of events decreases from 617 to 600. This decrease is consistent with the $\approx 3\%$ expectation obtained from Monte Carlo simulation [11].

We define four categories of dominant background events, all of which have missing transverse energy primarily arising from energy mismeasurement. We obtain the kinematic shapes and normalizations of each category separately. The four categories are (a) *misidentified photons*, referred to as ''misidentified γ,'' (b) *true photon plus light quark jet misidentified as heavy flavor*, referred to as ''true γ, misidentified b,'' (c) *true photon plus true b-quark jet*, referred to as ''γb,'' and (d) *true photon plus true c-quark jet*, referred to as ''γc.''

The misidentified γ background is estimated from the data sample itself by using cluster-shape variables from the CES and hit rates in the CPR. This technique (the CES/CPR method) allows the determination of the number of photon candidates in the sample that are actually misidentified jets as well as the corresponding shapes of the distributions of kinematic variables [30]. We describe the method in more detail in Sec. IV A.

The true γ plus misidentified b background is estimated by first selecting events that pass all cuts except the requirement of a b-tagged jet, resulting in 18 128 events (see Table I). For each selected event, we then apply the product of two weights: (i) the true-photon weight determined using the CES/CPR method, representing the probability that a photon candidate is a photon, and (ii) the heavy-flavor mistag [31] rate, which depends on jet E_T, jet η, the number of tracks in the jet, the number of primary interactions found in the event, and the z position of the primary interaction with the highest scalar sum p_T of tracks. The mistag parametrization is the same as that used in the measurement of the $t\bar{t}$ cross section [28]. Because the CES/CPR method and the mistag parametrization provide event-by-event weights, we are able to determine the shapes of kinematic distributions as well as the number of events for this background.

We estimate the γb and γc backgrounds by generating MC events using MADGRAPH [32] for leading-order matrix element processes involving photons, b or c quarks, and additional partons. The samples for $\gamma + b +$ jets and $\gamma + c +$ jets are generated with 1 to 3 jets. These samples are then processed with PYTHIA [33] to incorporate parton showering and hadronization. We ensure that we do not double count events due to the overlap between jets arising from matrix element partons and jets arising from initial and final state radiation [34]. We obtain the overall normal-

izations of these backgrounds by fitting the secondary vertex mass distribution of the tagged jets, $m(\mathrm{SV})$, to templates formed from the mass distributions of the expected SM components. The normalization scheme is described in Sec. IV B.

A summary of the background contributions is given in Table II.

A. Photon backgrounds: The CES/CPR method

For photon candidates with $E_T < 35$ GeV, we use the shape of the shower profile measured with the CES system to discriminate between true single photon events and diphoton final states from decays of mesons. We construct a χ^2 discriminant by comparing the measured shower profile with that measured in electron test beam data [30]. A single photon has an average probability of $\approx 78\%$ to satisfy the χ^2 cut, while the background has an average probability of $\approx 30\%$ to satisfy the χ^2 cut, since the shower profile of the two nearby photons from a meson decay is measurably wider on average.

Above 35 GeV, however, the two photons from meson decay coalesce and the discrimination power of the shower profile measurement is significantly reduced. In this E_T range, we use hit rates in the CPR system to discriminate between single photons and diphotons from meson decays. A single photon will convert and leave a hit in the preshower detector with a probability of $\approx 65\%$. Backgrounds that decay into two photons have a hit probability of $\approx 85\%$ because the probability that neither photon converts is lower than the probability that a single photon does not convert.

The difference of probabilities between signal (single photons) and background (photon pairs) forms the basis of a statistical method which assigns each event a weight for being a true photon (termed true-photon weight), $\mathcal{W}_\gamma$, as described in Ref. [30]. The weight is defined as

$$\mathcal{W}_\gamma = \frac{\delta_{\mathrm{candidate}} - \epsilon_{\mathrm{bkg}}}{\epsilon_{\mathrm{sig}} - \epsilon_{\mathrm{bkg}}}, \qquad (1)$$

where ϵ_{sig} and ϵ_{bkg} are the respective probabilities for a true photon and misidentified photon to satisfy a CES χ^2 cut or to leave a hit in the CPR, and $\delta_{\mathrm{candidate}}$ is either zero or 1 depending on whether the observed candidate satisfies these CES and CPR conditions. The values of ϵ_{sig} and ϵ_{bkg} are determined using control data samples [35] and are parametrized as a function of the energy of the photon candidate, the angle of incidence, and the number of primary interactions found in the event. The misidentified-photon weight is $1 - \mathcal{W}_\gamma$. We estimate the misidentified γ background by summing up the misidentified-photon weights of the 617 candidate events ($\gamma b j \not{E}_T$) to obtain 115 events with a statistical uncertainty of 49 events. We estimate the true γ, misidentified b background by summing up the products of true-photon weights and heavy-flavor mistag rates of the 18 128 events before the b-tagging selection ($\gamma j j \not{E}_T$) to obtain 141 events with a statistical uncertainty of six events. The calculation of the systematic uncertainty on these expectations is given in Sec. V.

B. Heavy-flavor normalization

The invariant mass of the tracks that form a secondary vertex can be used to discriminate between the bottom, charm, and light partons that compose a sample. We use this discriminating variable to normalize the contributions of the γb and γc backgrounds by fitting the secondary vertex mass distribution.

The fitting technique utilizes templates of the distribution of the secondary vertex mass arising from the three primary sources expected to contribute to the observed distribution: bottom quarks, charm quarks, and light quarks or gluons. These templates are obtained from Monte Carlo samples containing final state photons [36]. The discriminating power of the secondary vertex mass is shown in Fig. 1, in which the three templates are normalized to unit area [37]. The sum of the fractions of the three components is constrained to unity in the fit, $f_b + f_c + f_{\mathrm{light}} = 1$.

This technique can be used to determine the number of events containing a real photon and real heavy flavor in any sample. We first subtract the contribution due to misidentified photons by applying the CES/CPR method to obtain the number of misidentified photon events. We then estimate the fraction of heavy flavor in events with a misidentified photon by fitting the secondary vertex mass distribution in a sample enriched with jets faking photons, referred to as the *sideband* photon sample [38]. We then subtract the number of events containing a misidentified

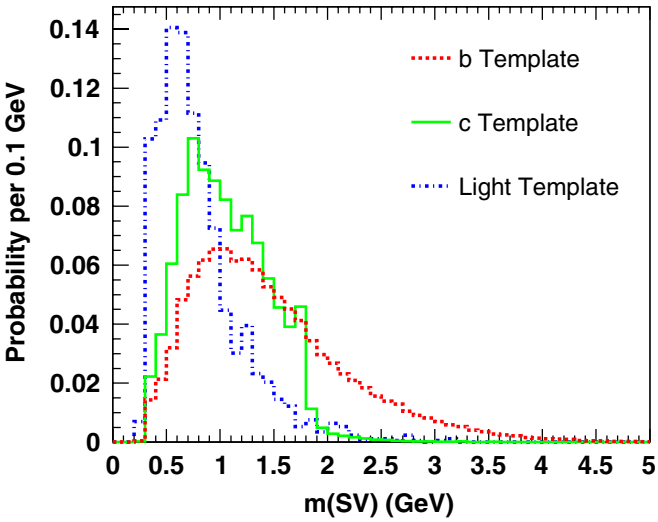

FIG. 1 (color online). Templates of the invariant mass of all tracks in a secondary vertex arising from bottom quarks, charm quarks, and light quarks and gluons from Monte Carlo simulations, normalized to unit area.

photon and heavy flavor from the number of events obtained from the standard photon sample fit to obtain the number of γb and γc events.

In principle, this technique could be directly applied to the search region to obtain the number of γb events. However, this would not give us the SM expectation, as the contribution from any new process making such events would be counted [39]. Instead, the expected γb contribution is normalized by applying this technique to a control region with a much larger SM cross section than that of the search region, and then extrapolating to the search region by using efficiencies derived from the $\gamma + b$ Monte Carlo simulation. The final estimate for the number of γb events in the search region is $N_{\gamma b}(\text{search}) = N_{\gamma b}(\text{control}) \cdot \varepsilon(\text{control} \rightarrow \text{search})$.

We define the control region as the $\gamma + b$-tag sample, where the only selection requirements are that there be at least one photon with $|\eta| < 1.1$ and $E_T > 25$ GeV and one SECVTX-tagged jet having $|\eta| < 2$ and $E_T > 15$ GeV. The number of events in the search region is less than 1% of that in the control region, which contains 93 894 events. We obtain an efficiency of $\varepsilon(\text{control} \rightarrow \text{search}) = 0.0123 \pm 0.0025$, defined as the fraction of $\gamma + b$ Monte Carlo events in the control region that survive the additional cuts of the search region. The uncertainty on the efficiency is due to the differences in jet multiplicities and $\not\!\!E_T$ distributions between data and the background prediction in the control region.

Figure 2 shows the results of a maximal likelihood fit performed on the search and control region using the templates above to extract the fraction of b-jet and c-jet events. We estimate the number of γb events by subtracting the misidentified photon plus b contribution from the control region and then multiplying by $\varepsilon(\text{control} \rightarrow \text{search})$ to obtain 341 events with a statistical uncertainty of 18 events. The calculation of the systematic uncertainty on the number of events is given in Sec. V.

The γc background is normalized by directly fitting the secondary vertex mass in the search region. We do not extrapolate the charm normalization from the control sample because the uncertainties on the matching scheme for charm quarks are large [40] and therefore the extrapolation efficiency would have large uncertainties. After subtracting the misidentified photon plus charm contribution, we obtain an estimate of nine γc events with a statistical uncertainty of $^{+52}_{-0}$ events.

Note that because the charm background is measured in the search region, this search is not sensitive to anomalous charm production. It is, however, sensitive to anomalous production of the $\gamma b j \not\!\!E_T$ final state because we use γb Monte Carlo processes to obtain the efficiency $\varepsilon(\text{control} \rightarrow \text{search})$.

V. SYSTEMATIC UNCERTAINTIES

Sources of systematic uncertainty on the number of predicted events arise from (a) the uncertainty on the true-photon weights $\mathcal{W}_\gamma$ in the CES/CPR method, (b) the uncertainty on the heavy-flavor mistag prediction, and (c) the uncertainty on the template shapes used in the secondary vertex mass fit.

The systematic uncertainty on $\mathcal{W}_\gamma$ in the CES/CPR method arises from uncertainties on the CES χ^2 efficiencies and the CPR hit rates for photons and backgrounds [ϵ_{sig} and ϵ_{bkg} in Eq. (1)]. The largest uncertainty on the CES χ^2 efficiencies is due to the gain saturation in the CES detector [30] (10% on $\mathcal{W}_\gamma$). The largest uncertainty on the CPR hit rates is due to the modeling of the hit rates of π^0 and η^0 (5%–35% on $\mathcal{W}_\gamma$). On average, $\mathcal{W}_\gamma$ has a relative systematic uncertainty of 11%.

The uncertainty on the heavy-flavor mistag prediction comes from the finite size of data samples used for parametrization of the mistag rates (10%), variations between different data-taking periods (6.5%), and the uncertainty on

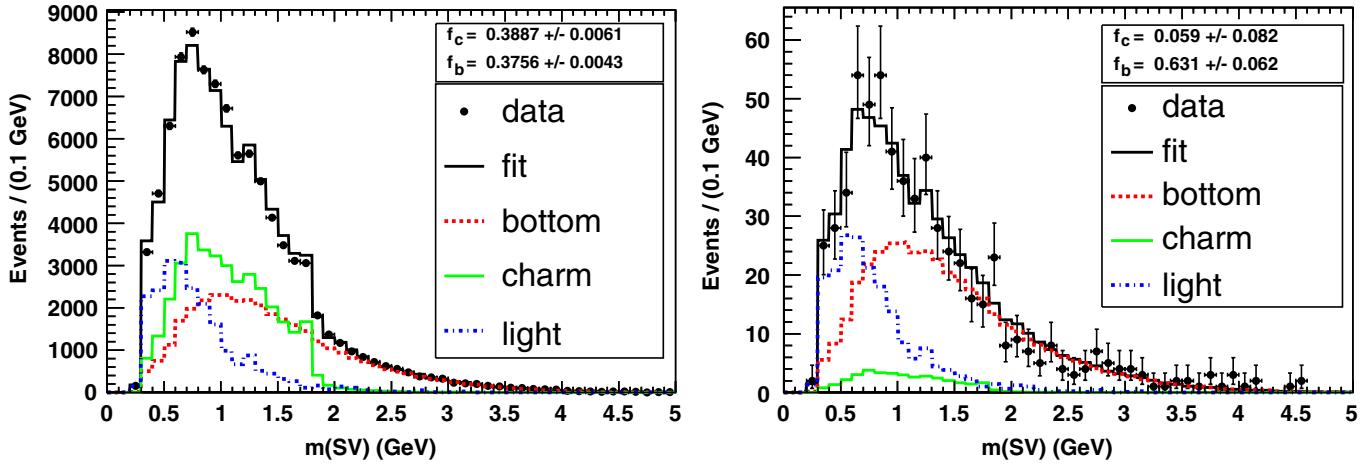

FIG. 2 (color online). The secondary vertex mass fit in events containing standard photons, for the control sample (left panel) and the search sample (right panel). Note the uncertainties on f_c and f_b are correlated and purely statistical.

a scale factor which takes into account the contribution of misidentified b-tags from long-lived hadrons (Λ^0, K_s^0) and secondary particles due to interactions with detector material (10%–15%). More details may be found in Ref. [28].

We estimate the systematic uncertainty arising from the secondary vertex mass fitting procedure by varying the shapes of the templates that are used in the binned likelihood fit. The systematic effect of mismodeled tracking inefficiency in the Monte Carlo simulation is estimated by lowering the secondary vertex mass template mass scale by 3% [41]. We also refit the secondary vertex mass distributions with templates derived from Monte Carlo samples that have the $\not\!\!E_T > 25$ GeV cut imposed on them, as this may change the relative fraction of semileptonic decays in the template samples and thereby alter the secondary vertex mass distribution. Because both of these sources of uncertainty affect the shape of the templates, we take the maximum variation observed as the systematic shift in normalization. We obtain a 12% uncertainty on the b fraction and a 48% uncertainty on the c fraction from this estimate.

The numerical values of the systematic uncertainties are presented in Table II in Sec. VI below. The CES/CPR method contributes 13% of the systematic uncertainty on the total amount of background, while the mistag parametrization and secondary vertex mass fit contribute 24% and 63%, respectively. The calculation of the total systematic uncertainty takes into account correlations among the different sources of backgrounds to the $\gamma bj\not\!\!E_T$ signature. Because the CES/CPR method is used to estimate the contribution of all four background categories defined in Sec. IV, we apply the CES/CPR systematic variations to all backgrounds simultaneously when calculating the final CES/CPR uncertainty on the total background prediction. All other sources of systematic uncertainty are combined as uncorrelated uncertainties.

VI. RESULTS

We proceed to test the SM in the $\gamma bj\not\!\!E_T$ signature in three ways: comparing predicted event counts, looking for anomalous kinematic behavior, and counting additional objects in the events, as might be expected from the production of new heavy states with extended decay chains. We also go beyond the run I measurement criteria by increasing the requirement on missing transverse energy to 50 GeV, reducing the expected background contribution by a factor of ≈ 20, and thereby enhancing the sensitivity to new processes. The three tests are described in the sections below.

A. Comparing predicted event counts

Table II summarizes the background sources with associated statistical and systematic uncertainties. The total background prediction is

TABLE II. The numbers of predicted events from background sources. The two uncertainties in each row are statistical and systematic, respectively. Note that the total systematic uncertainty is less than the largest individual contribution due to an anticorrelation of the CES/CPR uncertainties between the components.

Background source	Expected events	Statistical	Systematic
Misidentified γ	115	± 49	± 54
True γ, misidentified b	141	± 6	± 30
γb	341	± 18	± 91
γc	9	± 52	± 14
Total	607	± 74	± 86

$$N(\mathrm{BG}) = 607 \pm 74(\mathrm{stat}) \pm 86(\mathrm{syst}), \quad (2)$$

where the first uncertainty is statistical and the second systematic. The observed number of events is 617, consistent with the background predictions.

B. Object kinematics

We examine three different types of distributions for anomalous shape discrepancies with respect to the background prediction: the kinematics of individual objects in the event such as jets and photons, global features of the event such as $\not\!\!E_T$, and the invariant masses of the combinations of objects.

The distributions of the transverse energy of the photon, the b-jet, and the 2nd jet are shown in Figs. 3–5, respectively. The distributions of E_T, N(jets), and H_T, where H_T is the scalar sum of the transverse momenta of the photon, all jets in the event, and $\not\!\!E_T$ are shown in Figs. 6–8, respectively. The $\not\!\!E_T$ distribution is shown before the application of the $\not\!\!E_T > 25$ GeV cut but after the application of all other selections. The distributions of $M(\gamma b)$, $M(bj)$,

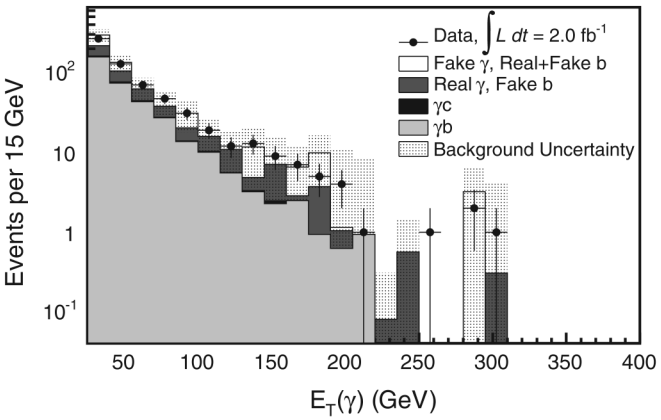

FIG. 3. The distribution in photon E_T observed (points) and from backgrounds (histogram). The KS p-value is 63.7%. Note that the single event in a bin that has no predicted background is due to the choice of binning and is therefore not a significant excess.

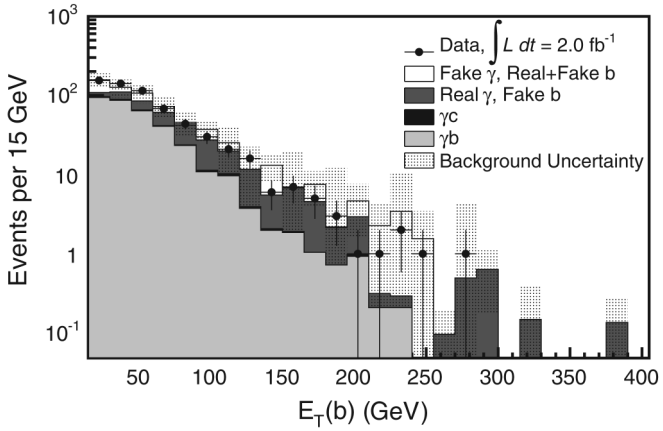

FIG. 4. The distribution in the b-jet E_T observed (points) and from backgrounds (histograms). The KS p-value is 59.7%.

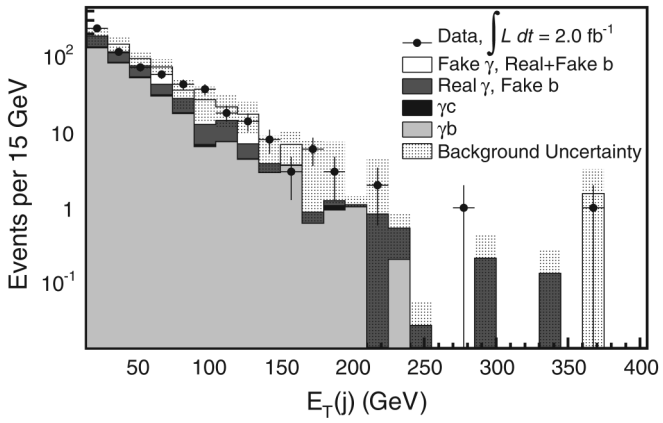

FIG. 5. The distribution in the untagged jet E_T observed (points) and from backgrounds (histogram). The KS p-value is 10.4%. Note that the single event in a bin that has no predicted background is due to the choice of binning and is therefore not a significant excess.

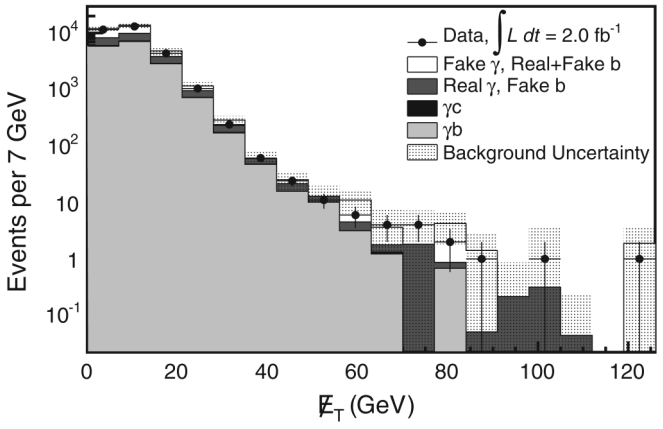

FIG. 6. The distribution in missing transverse energy observed (points) and from backgrounds (histogram). The KS p-value is 7.0%.

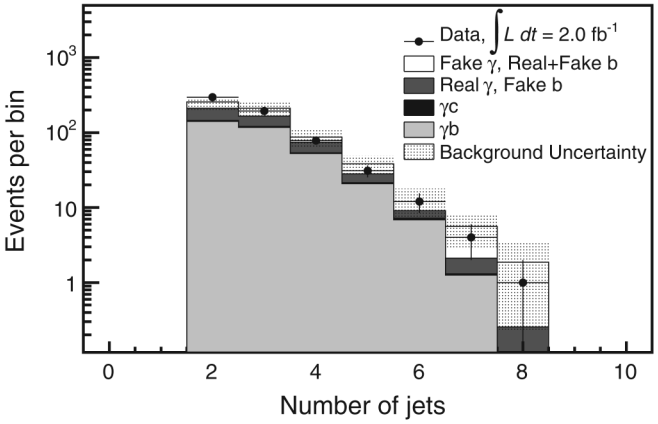

FIG. 7. The distribution in jet multiplicity observed (points) and from backgrounds (histogram) in the logarithmic scale. The KS p-value is 19.0%.

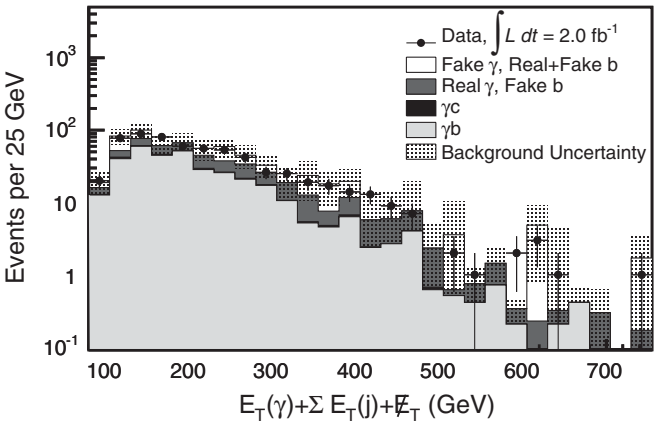

FIG. 8. The distribution of the scalar sum of the transverse momenta of the γ, all jets in the event, and $\not\!\!E_T$ observed (points) and from backgrounds (histogram). The KS p-value is 99.7%.

$M(\gamma bj)$, $M_T(\gamma \not\!\!E_T)$, and $M_T(bj \not\!\!E_T)$ are shown in Figs. 9–13, respectively. The transverse mass M_T is calculated with the transverse components of object momenta:

$$M_T = \sqrt{(\Sigma_i E_T^i)^2 - (\Sigma_i p_x^i)^2 - (\Sigma_i p_y^i)^2}, \qquad (3)$$

where E_T^i, p_x^i, and p_y^i are the transverse energy and x and y components of the momentum of object i (which could be a photon, b-quark jet, jet, or missing energy). Note that the binning for all distributions is such that there are no overflows.

We test the consistency between the observed shapes of kinematic distributions and the shape predicted by the background expectation by running pseudoexperiments for each distribution studied and calculating the Kolmogorov-Smirnov (KS) distance for each pseudoexperiment. The use of pseudoexperiments corrects for biases that can occur when using binned data to calculate the KS distance. The probability that a random sampling of the

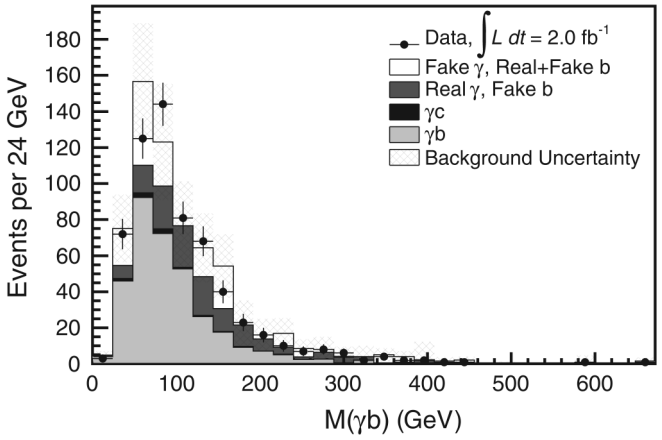

FIG. 9. The distribution of the mass of the photon + b jet observed (points) and from backgrounds (histogram). The KS p-value is 62.0%.

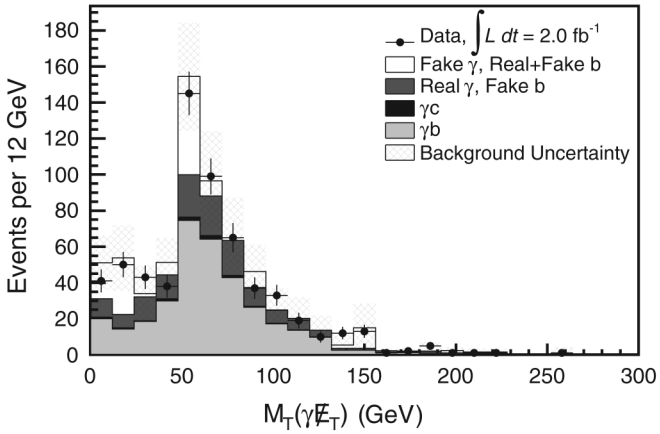

FIG. 12. The distribution of the transverse mass of the photon + $\not\!\!E_T$ observed (points) and from backgrounds (histogram). The KS p-value is 96.8%.

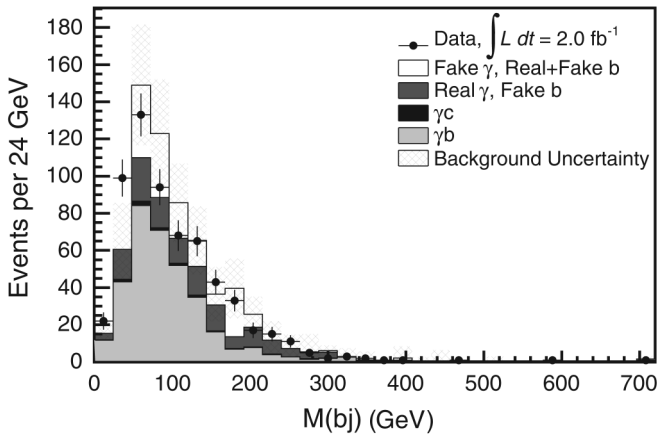

FIG. 10. The distribution of the dijet mass observed (points) and from backgrounds (histogram). The KS p-value is 9.8%.

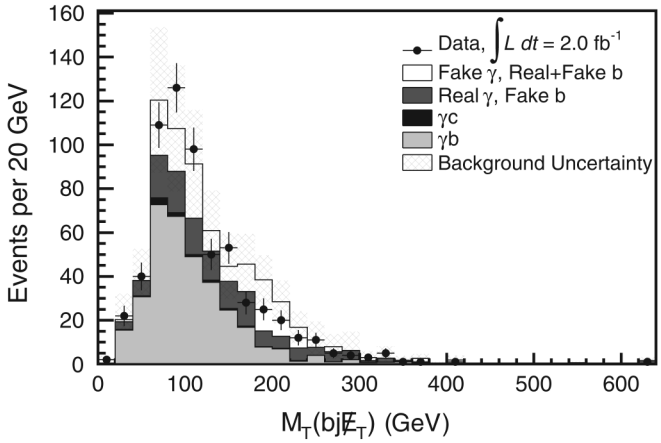

FIG. 13. The distribution of the transverse mass of the b jet, the 2nd jet, and missing transverse energy observed (points) and from backgrounds (histogram). The KS p-value is 21.1%.

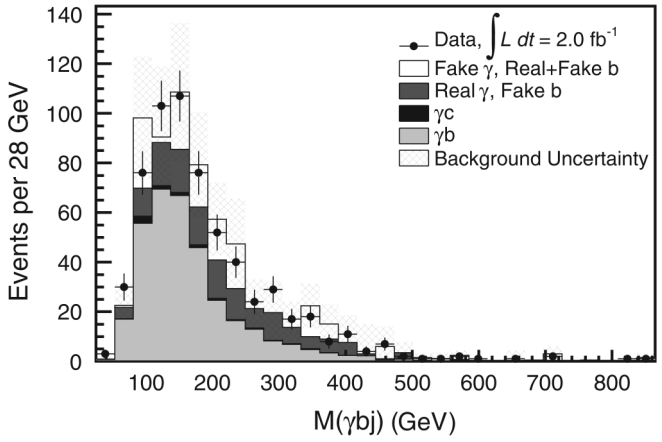

FIG. 11. The distribution of the invariant mass of the γ, the b jet, and the 2nd jet observed (points) and from backgrounds (histogram). The KS p-value is 99.8%.

estimated background distribution would give a higher KS distance than the observed data distribution, referred to as the "KS p-value," is obtained for each kinematic variable studied by integrating the tail of the distribution of KS distances. We obtain a range of KS p-values between 7.0% and 99.8%, indicating that the kinematic distributions observed are consistent with background expectations.

C. Effect of additional selections

We further investigate the existence of possible anomalies in the $\gamma b j \not\!\!E_T X$ final state by making additional selections and comparing the number of observed events to the background predictions. We chose criteria based on expected SM distributions and selections used previously in the search of Ref [10]. The additional selections we make are $\not\!\!E_T > 50$ GeV, $N(\text{jets}) \geq 3$, $p_T(\gamma) > 50$ GeV, $H_T > 200$ GeV, $E_T(b) > 50$ GeV, and $\Delta\phi(\text{jet}, \not\!\!E_T) > 0.5$.

TABLE III. The number of events observed and the predicted background for additional independent selections. The first uncertainty in the observed columns is statistical and the second is systematic.

Selection	No additional cuts		With $\not\!\!E_T > 50$ GeV	
	Observed	Predicted	Observed	Predicted
$\not\!\!E_T > 50$ GeV	28	$30 \pm 10 \pm 5$		
$N(\text{jets}) \geq 3$	321	$329 \pm 46 \pm 46$	15	$17 \pm 7 \pm 3$
$p_T(\gamma) > 50$ GeV	257	$247 \pm 42 \pm 39$	16	$21 \pm 8 \pm 5$
$H_T > 200$ GeV	304	$322 \pm 45 \pm 46$	25	$28 \pm 9 \pm 5$
$E_T(b) > 50$ GeV	286	$310 \pm 43 \pm 44$	18	$22 \pm 8 \pm 6$
$\Delta\phi(\text{jet}, \not\!\!E_T) > 0.5$	343	$368 \pm 47 \pm 49$	15	$16 \pm 8 \pm 4$

Table III summarizes the effects of the additional selections. We apply these in two different ways: one at a time independently of all other additional selections, and after the application of the $\not\!\!E_T > 50$ GeV selection. No anomalous excess of events is observed.

Finally, exotic particles with cascade decays, $X \rightarrow \gamma Y \rightarrow bj$, may form a cluster in the scatter plot of $M(\gamma bj)$ vs $M(bj)$. In Fig. 14, we compare the observed distribution to that from the estimated background; we do not see any evidence of an anomaly.

D. Efficiencies for setting limits

To allow the calculation of a limit on a model of physics beyond that in the SM, we provide the efficiencies and acceptances needed as inputs to the limit estimating procedure for signature-based searches described in Ref. [10]. This method requires that a distinction be made between acceptance, A, which we take as the probability that an object passes kinematic, geometric, and fiducial cuts, and the efficiency, ϵ, which is the probability of the event surviving all other detector-specific sources of inefficiency. The acceptance may be calculated from kinematic and geometric criteria alone, while the efficiency requires access to a detector simulation.

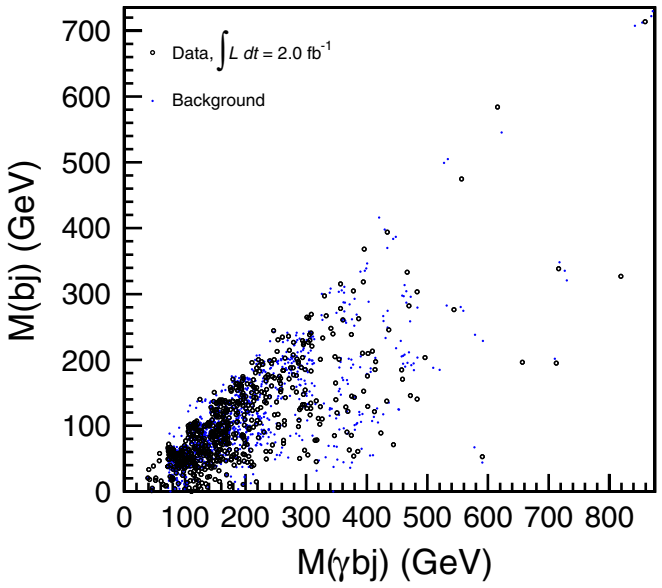

FIG. 14 (color online). $M(bj)$ versus $M(\gamma bj)$ for the events which satisfy the selections in Table I, observed (big dots) and expected (small dots).

The acceptance criteria for this analysis are presented in Sec. III. The corresponding efficiencies are for the photon (ϵ_γ), the b-quark tag (ϵ_b), the jet (ϵ_j), and $\not\!\!E_T$ ($\epsilon_{\not\!\!E_T}$). The photon identification efficiency is measured with $Z \rightarrow e^+e^-$ events, using electrons that are fiducial to the CES. For an isolated, accepted ($|\eta| < 1$, $E_T > 25$ GeV) photon the probability that it passes CES fiducial and identification cuts is $\epsilon_\gamma = 64\%$. For models with partons in the accepted region of jet pseudorapidity, $|\eta| < 2$, and well over the E_T selection threshold, $E_T > 15$ GeV, the jet selection efficiency is approximately 100%. Similarly, for models with large intrinsic $\not\!\!E_T$, the $\not\!\!E_T$ resolution does not have a measurable effect on the efficiency to select $\not\!\!E_T > 25$ GeV. We therefore quote the efficiency to reconstruct jets and $\not\!\!E_T$ after the application of kinematic acceptances to be $\epsilon_{\text{jet}} = \epsilon_{\not\!\!E_T} = 100\%$. The b-tagging efficiency is calculated to be $\epsilon_b = (39 \pm 1)\%$ [28]. The total efficiency for the final state is then $\epsilon_{\text{event}} = \epsilon_\gamma \times \epsilon_b = 25\%$. It should be noted that limits obtained via this technique do not take correlations between objects into account. Previous studies have shown that limits calculated in this way can have uncertainties in the range of 3%–45% [10].

VII. CONCLUSIONS

We have searched for the anomalous production of events containing a photon, two jets (one which is identified as originating from a b quark), and missing transverse energy. The number of events observed in data is consistent with the number of expected background events. No significant excess of events with respect to the background prediction is observed in any of the kinematic distributions studied. The shapes of these distributions are consistent with SM expectations. Furthermore, we do not see any anomalous production of events after applying additional selections. We conclude that the 2.0 ± 0.1 fb^{-1} $\gamma + b + j + \not\!\!E_T + X$ sample is consistent with SM background expectations.

ACKNOWLEDGMENTS

We thank Stephen Mrenna for teaching us how to implement the matching of matrix element n-jet channels. We also would like to thank Zack Sullivan for helpful discussions and Michel Herquet and Johann Alwall for providing resources and support for MADGRAPH. We thank the Fermilab staff and the technical staffs of the participating institutions for their vital contributions. This work was supported by the U.S. Department of Energy and National Science Foundation; the Italian Istituto Nazionale di Fisica Nucleare; the Ministry of Education, Culture, Sports, Science and Technology of Japan; the Natural Sciences and Engineering Research Council of Canada; the National Science Council of the Republic of China; the Swiss National Science Foundation; the A. P. Sloan Foundation; the Bundesministerium für Bildung und Forschung, Germany; the Korean Science and Engineering Foundation and the Korean Research Foundation; the Science and Technology Facilities Council and the Royal Society, United Kingdom; the Institut National de Physique Nucleaire et Physique des Particules/CNRS; the Russian Foundation for Basic Research; the Ministerio de Ciencia e Innovación, and Programa Consolider-Ingenio 2010, Spain; the Slovak R&D Agency; and the Academy of Finland.

[1] F. Abe *et al.*, Nucl. Instrum. Methods **271**, 387 (1988); D. Acosta *et al.* (CDF Collaboration), Phys. Rev. D **71**, 052003 (2005); The CDF II Detector Technical Design Report, Fermilab-Pub-96/390-E; A. Abulencia *et al.* (CDF Collaboration), J. Phys. G **34**, 2457 (2007); T. Aaltonen *et al.* (CDF Collaboration), Phys. Rev. D **77**, 112001 (2008).

[2] The CDF II detector uses a cylindrical coordinate system in which ϕ is the azimuthal angle, r is the radius from the nominal beam line, and z points in the proton beam direction. The transverse $(r-\phi)$ plane is perpendicular to the z axis. Transverse momentum and energy are the respective projections of momentum measured in the tracking system and energy measured in the calorimeter system onto the $r-\phi$ plane, and are defined as $p_T = p\sin\theta$ and $E_T = E\sin\theta$. Here, θ is the polar angle measured with respect to the interaction vertex. Missing E_T ($\vec{\not\!\!E}_T$) is defined by $\vec{\not\!\!E}_T = -\sum_i E_T^i \hat{n}_i$, where i is the calorimeter tower number for $|\eta| < 3.6$, and $\hat{n}_i$ is a unit vector perpendicular to the beam axis and pointing at the ith tower. The pseudorapidity η is defined as $-\ln(\tan(\theta/2))$, where θ is measured with respect to the origin of the detector. We define the magnitude $\not\!\!E_T = |\vec{\not\!\!E}_T|$. We use the convention that "momentum" refers to pc and "mass" to mc^2.

[3] F. Abe *et al.* (CDF Collaboration), Phys. Rev. D **59**, 092002 (1999); F. Abe *et al.* (CDF Collaboration), Phys. Rev. Lett. **81**, 1791 (1998).

[4] D. Acosta *et al.* (CDF Collaboration), Phys. Rev. D **66**, 012004 (2002); Phys. Rev. Lett. **89**, 041802 (2002); J. Berryhill, Ph.D. thesis, University of Chicago, 2000.

[5] D. Acosta *et al.* (CDF Collaboration), Phys. Rev. Lett. **89**, 281801 (2002).

[6] A. Abulencia *et al.* (CDF Collaboration), Phys. Rev. Lett. **97**, 031801 (2006); Phys. Rev. D **75**, 112001 (2007).

[7] A. Abulencia *et al.* (CDF Collaboration), Phys. Rev. Lett. **99**, 121801 (2007).

[8] T. Aaltonen *et al.* (CDF Collaboration) (unpublished).

[9] T. Aaltonen *et al.* (CDF Collaboration), Phys. Rev. D **78**, 012002 (2008); Phys. Rev. D **79**, 011101 (2009).

[10] T. Affolder *et al.* (CDF Collaboration), Phys. Rev. D **65**, 052006 (2002).

[11] This expectation is based on the simulation of the listed SM processes and subsequent application of the analysis code. The $t\bar{t}$ sample is generated using the PYTHIA generator [33]. The $Wb\bar{b}$ and $Zb\bar{b}$ samples are generated using the ALPGEN event generator interfaced with PYTHIA as a parton shower. Details of the ALPGEN generator may be found in M. L. Mangano, M. Moretti, F. Piccinini, R. Pittau, and A. D. Polosa, J. High Energy Phys. 07 (2003) 001.

[12] A. Sill *et al.*, Nucl. Instrum. Methods **447**, 1 (2000); A. Affolder *et al.*, Nucl. Instrum. Methods **453**, 84 (2000); C. S. Hill *et al.*, Nucl. Instrum. Methods **530**, 1 (2004).

[13] A. Affolder *et al.*, Nucl. Instrum. Methods **526**, 249 (2004).

[14] L. Balka *et al.*, Nucl. Instrum. Methods **267**, 272 (1988).

[15] S. Bertolucci *et al.*, Nucl. Instrum. Methods **267**, 301 (1988).

[16] S. Kuhlmann *et al.*, Nucl. Instrum. Methods **518**, 39 (2004).

[17] F. Abe *et al.* (CDF Collaboration), Phys. Rev. Lett. **68**, 1104 (1992).

[18] G. Ascoli *et al.*, Nucl. Instrum. Methods **268**, 33 (1988); A. Artikov *et al.*, Nucl. Instrum. Methods **538**, 358 (2005).

[19] D. Acosta *et al.* (CDF Collaboration), Nucl. Instrum. Methods **461**, 540 (2001); **494**, 57 (2002).

[20] D. Acosta *et al.* (CDF Collaboration), Phys. Rev. Lett. **94**, 091803 (2005).

[21] F. Abe *et al.* (CDF Collaboration), Nucl. Instrum. Methods **271**, 387 (1988).

[22] The trigger requires one electromagnetic (EM) cluster with (i) $E_T > 25$ GeV and (ii) isolation energy less than 2 GeV or $0.1 \times E_T$. The energy of the EM cluster is the sum of the energies measured in two adjacent calorimeter towers at the same wedge, i.e. $\Delta\phi \times \Delta\eta \approx 15^\circ \times 0.2$. The isolation energy is calculated as the sum of E_T of all towers (except for the EM cluster) in the cone with radius $R = 0.4$ centered around the EM cluster.

[23] D. Acosta *et al.* (CDF Collaboration), Phys. Rev. D **71**, 031104 (2005).
[24] F. Abe *et al.* (CDF Collaboration), Phys. Rev. D **52**, 4784 (1995); D. Acosta *et al.* (CDF Collaboration), Phys. Rev. D **65**, 112003 (2002).
[25] The ratio of hadronic energy to electromagnetic energy, $E_{\rm had}/E_{\rm em}$, must be less than $0.055 + 0.000\,45 \times E_{\rm em}$ (GeV).
[26] F. Abe *et al.* (CDF Collaboration), Phys. Rev. D **45**, 1448 (1992).
[27] A. Bhatti *et al.*, Nucl. Instrum. Methods **566**, 375 (2006).
[28] D. Acosta *et al.* (CDF Collaboration), Phys. Rev. D **71**, 052003 (2005); C. Neu, Report No. FERMILAB-CONF-06-162-E, 2006.
[29] Tracks with $p_T > 500$ MeV are included in the isolation sum, $\sum_i p_T^i$, if they are in a cone of size $\Delta R = 0.4$ around the isolated track candidate, have greater than 23(19) axial (stereo) hits in the tracking chamber, and have a beam-corrected track impact parameter $|d_0| < 250$ μm. In addition, they are required to have ≥ 3 silicon hits on the track if the number expected is ≥ 3, and a difference of the z component of closest approach to the primary vertex of $|z_i - z_{\rm track}| < 5$ cm with $|z_{\rm track}| < 60$ cm.
[30] F. Abe *et al.* (CDF Collaboration), Phys. Rev. D **48**, 2998 (1993).
[31] The heavy-flavor mistag rate is the probability that a light quark or gluon jet will be misidentified as heavy flavor by the SECVTX algorithm. This rate is of order 1%.
[32] J. Alwall, P. Demin, S. de Visscher, R. Frederix, M. Herquet, F. Maltoni, T. Plehn, D. L. Rainwater, and T. Stelzer, J. High Energy Phys. 09 (2007) 028.
[33] T. Sjöstrand, S. Mrenna, and P. Skands, J. High Energy Phys. 05 (2006) 026.
[34] J. Alwall *et al.*, Eur. Phys. J. C **53**, 473 (2008); S. Mrenna (private communication).
[35] The values of $\epsilon_{\rm sig}$ and $\epsilon_{\rm bkg}$ are first determined from the standard CDF simulation of single photons and a mixture of mesons according to their relative productions and reconstruction efficiencies, where the CES and CPR responses are tuned based on electron test beam and W leptonic decays. We then calibrate $\epsilon_{\rm sig}$ with a pure photon sample obtained from $W^- \to \ell^- \bar{\nu}_\ell \gamma$ and $Z^0 \to \ell^+ \ell^- \gamma$ decays. The efficiency for background, $\epsilon_{\rm bkg}$, is calibrated using the isolation distribution of inclusive photon candidates.
[36] Because the event topology of photon events may be different from that of generic multijet events, we use templates that are derived from samples containing true photons. The bottom and charm templates are obtained from MADGRAPH samples as described in Sec. IV and the light template is obtained from a PYTHIA inclusive photon sample with the heavy flavor removed.
[37] The feature in the charm template near $m(\mathrm{SV}) = 1.8$ GeV$/c^2$ is attributable to D^0 and D^+ decays, where the invariant mass of the constituent tracks almost reproduces the mass of the decaying hadron. This peak is prominent because the D^0 and D^+ hadrons are the most common components of charm jets.
[38] The sideband-photon candidates satisfy loose identification requirements but fail the standard requirements as described in Ref. [23]. The loose photon identification has reduced requirements on the shower profile, leakage into the hadron calorimeter, and isolation. It has been estimated that only $\approx 5\%$ of the sideband-photon sample has true photons.
[39] Applying this secondary mass fit technique to the search sample gives 325 ± 40 γb events, compared to the prediction obtained directly from the control sample of 341 ± 18 events, where the uncertainties are statistical only.
[40] Z. Sullivan (private communication).
[41] This is derived from comparisons of tracking efficiency between Monte Carlo simulation and data. The effect of possible mismodeling is then propagated to the mass of secondary vertices.